npj computational materials

www.nature.com/npjcompumats

ARTICLE OPEN

Symmetry-driven half-integer conductance quantization in Cobalt–fulvalene sandwich nanowire

Zhuoling Jiang[1,2,5], Kah-Meng Yam[1,3,5], Yee Sin Ang[2]✉, Na Guo[4], Yongjie Zhang[1], Hao Wang[1] and Chun Zhang[1,3,4]✉

Precise manipulation and monitoring spin transport in one-dimensional (1D) systems is a long-sought goal in the field of nano-spintronics. Based on first-principles calculations, we report the observation of half-integer conductance quantization in the Cobalt-fulvalene sandwich nanowire. Compared with a pure monatomic Cobalt wire, the introduction of fulvalene molecules leads to three important features: Firstly, the strong coupling between the fulvalene and the Cobalt prevents the contamination of the ambient air, ensuring both chemical and physical stabilities; Secondly, the fulvalene symmetry-selectively filters out most of the *d*-type orbitals of the Cobalt while leaving a single *d*-type orbital to form an open spin channel around the Fermi level, which offers a mechanism to achieve the observed half-integer conductance; Thirdly, it maintains a superexchange coupling between adjacent Co atoms to achieve a high Curie temperature. Spin transport calculations show that this half-metallic nanowire can serve as a perfect spin filter or a spin valve device, thus revealing the potential of Cobalt-fulvalene sandwich nanowire as a promising building block of high-performance spintronics technology.

npj Computational Materials (2023)9:198 ; https://doi.org/10.1038/s41524-023-01151-z

INTRODUCTION

One-dimensional (1D) monatomic metals or molecular nanowires have attracted tremendous interest in recent decades owing to their promising potential for next-generation nanoelectronics[1–23]. The quantization of their conductance in multiple units of $G_0 = 2e^2/h$ is a signature of ballistic transport in a 1D nanowire. Previous studies have demonstrated that noble metals, such as Au, Ag, and Cu, can exhibit quantum conductance of $1G_0$ in the monatomic wires, which is indicative of a single-spin-degenerate channel[24–26]. When the metallic nanowire is magnetic, a half-integer conductance of $0.5G_0$ may be observed because of the lifted spin degeneracy, suggesting a single-spin channel. Enormous efforts have been devoted to the search for 1D magnetic nanowires that exhibit a half-integer conductance, as it simplifies the processes of the production, detection, and manipulation of fully spin-polarized current. For instance, detecting the spin current can be accomplished by simply measuring a half-integer quantized conductance plateau, without the need of sophisticated techniques, such as an external magnetic field or top-gate bias[2,11,15]. Furthermore, benefiting from the potential to precisely control and monitor spin transport in a single-spin channel, these 1D magnetic systems can be utilized for versatile applications, including spin-qubit quantum computer[27], spin filter[28–31], and magnetic random access memory[32,33].

Rodrigues et al. first observed half-integer conductance in a monatomic Co nanowire and claimed that such an effect originated from a single fully spin-polarized channel[2]. However, subsequent experimental and theoretical studies questioned this outcome[34–44], and argued, instead, that the $0.5G_0$ conductance may be caused by the contamination of H_2 in the Co nanowire[37]. For most transition metal wires, many *d* bands cross the Fermi level in both majority and minority spin channels, and thus a complete spin polarization appears to be impossible[34–36,38–44]. Furthermore, from a practical point of view, monatomic metal wire is inherently unstable and readily contaminated by ambient gas. Consequently, many researchers have redirected their attention to exploring other 1D systems, such as 1D organic, organometallic, and inorganic nanowires. Although several experimental works have claimed the observation of half-integer conductance in 1D quantum systems[5,15,45], they relied heavily on sophisticated techniques to create a single-spin channel, such as an external magnetic field or gate voltage. For instance, 1D GaAs nanowire, through the modulation of top-gate bias, would exhibit a half-integer quantum conductance[5]. Theoretical studies have proposed that 1D multidecker organometallic sandwich molecular wires (SMWs) can exhibit half-metallicity property with a single *d* band crossing the Fermi level, e.g., $(MnBz)_\infty$[7,9], $(VCp)_\infty$[9,10] and $(CoH_3)_\infty$[21]. However, because of the high-symmetry structure of SMWs, this *d* band is actually a two-fold degenerate band *e1* (d_{xz}, d_{yz}) or *e2* (d_{xy}, $d_{x^2-y^2}$), resulting in two ballistic conductance channels. In other words, these SMWs still exhibit an integer conductance quantization of $1G_0$. To date, the existence of a 1D nanowire that intrinsically displays a half-integer conductance without utilizing sophisticated techniques remains an unsolved puzzle.

In this work, we have proposed that 1D SMW composed of Cobalt atoms and fulvalene ($C_{10}H_8$) molecules, referred to as $(CoFul)_\infty$, can exhibit a half-integer conductance quantization of $0.5\ G_0$. Our calculations demonstrate that the introduction of fulvalene enhances the physical and chemical stabilities of the $(CoFul)_\infty$ nanowire. In addition, the fulvalene provides a mechanism of symmetry-selective filtering, which creates a single-spin channel responsible for the half-integer conductance quantization. Besides, this $(CoFul)_\infty$ nanowire favors a ferromagnetic ground state with a magnetic moment of $1\mu_B$ localized at the Co atom, which may serve as a perfect 1D Ising spin-1/2 chain[46].

[1]Department of Physics and Centre for Advanced 2D Materials, National University of Singapore, Singapore 117551, Singapore. [2]Science, Mathematics and Technology (SMT) Cluster, Singapore University of Technology and Design, Singapore 487372, Singapore. [3]Department of Chemistry, National University of Singapore, Singapore 117543, Singapore. [4]National University of Singapore Chongqing Research Institute, 401123 Chongqing, China. [5]These authors contributed equally: Zhuoling Jiang, Kah-Meng Yam. ✉email: yeesin_ang@sutd.edu.sg; phyzc@nus.edu.sg

When arranged in a 2D nanowire array, the $(CoFul)_\infty$ exhibits a high Curie temperature of 267 K, making it feasible for room-temperature applications. With exceptional features above, the $(CoFul)_\infty$ nanowire offers an invaluable platform for verifying previously proposed fundamental theories, such as the quantum communication protocol through single-spin-qubit transiting in 1D ferromagnet[47], single-spin inelastic tunneling spectroscopy[48,49] and spin dynamics theory of 1D Ising single-spin chain[50–53]. Furthermore, a class of $(TMFul)_\infty$ nanowires, derived from the $(CoFul)_\infty$, exhibit a broad range of electronic and magnetic properties, holding great potential for multifunctional spintronics applications. To showcase this potential, we have designed a molecular magnetic tunneling junction (MTJ)[31] utilizing the $(CoFul)_\infty$ nanowire. Benefiting from the spin transmitting confined in a single open spin channel, this MTJ exhibits exceptional performance, with an impressive spin filter efficiency (SFE) of nearly 100% and a staggering tunneling magneto-resistance (TMR) of up to ~10^7%. To the best of our knowledge, these outcomes represent the best record in the field of molecular MTJs thus far.

RESULTS

Stability of 1D $(CoFul)_\infty$ nanowire and feasibility of experimental design

Prior to showcasing the features of 1D $(CoFul)_\infty$ nanowire, we first elucidate why a pure monatomic Co nanowire fails to give a complete spin current. The optimized lattice constant of the Co nanowire is 2.16 Å, as shown in Fig. 1a, and two initial magnetic configurations are taken into account for a double-unit-cell containing two Co atoms: ferromagnetic state (FM) and antiferromagnetic state (AFM). Consistent with previous works[1,36,41,43,54], the Co nanowire favors the FM phase, having an exchange energy ($\Delta E_{ex} = E_{AFM} - E_{FM}$) of 0.98 eV and a magnetic moment of 2.13 μ_B per Co atom. The conductivity of the Co nanowire can be described by the Landauer formula $G = G_0/2\sum_{n,\sigma} T_{n,\sigma}$, where $T_{n,\sigma}$ is the transmission coefficient of the nth conduction channel for a spin σ. Generally, under the ballistic regime, the conductance can be determined directly by counting the total number of conduction channels, i.e., the total number of dispersive bands crossing the Fermi level. As shown in Fig. 1b, the spin-polarized band structure of the Co nanowire reveals that the bands near the Fermi level are primarily dominated by the d orbitals of Co. Only one ballistic conductance channel, arising from the hybridization of s orbital and d_{z^2} orbital, is present for the majority spin, yielding a conductance of $G_0/2$. For the minority spin, six ballistic conductance channels exist, stemming from the degenerate d_{xz} and d_{yz} orbitals, the degenerate d_{xy} and $d_{x^2-y^2}$ orbitals, and two s-d_{z^2} hybridized orbitals. These conductance channels collectively result in a total conductance of $3.5G_0$. Due to the co-contribution of both the majority and minority spins, the electrons propagating along the Co nanowire are not fully spin-polarized.

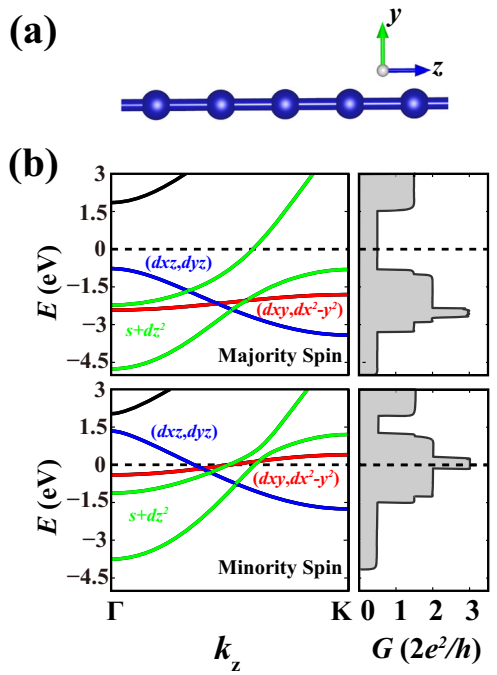

Fig. 1 The atomic structure and electronic and transport properties of the Co nanowire. a The optimized atomic structure of 1D Co nanowire and **b** the corresponding spin-polarized band structure and tunneling conductance.

To attain a complete spin-polarized current, a fulvalene molecule ($C_{10}H_8$) is inserted between two adjacent Co atoms in the Co nanowire, therefore generating a Cobalt-fulvalene sandwich nanowire, referred to as $(CoFul)_\infty$. This arrangement is made possible in the experiment, as demonstrated in previous experimental works[55], that a planer fulvalene ligand linking two metal atoms will emerge after fusing two metallocene ($M(C_5H_5)_2$) molecules. Moreover, a recent experiment[56] has successfully synthesized metallocene polymers with more than two metallocene molecules. Drawing on similar strategies, it is feasible to experimentally fabricate a 1D $(CoFul)_\infty$ nanowire by polymerizing Cobaltocene ($Co(C_5H_5)_2$) molecules (Fig. 2a). The optimized lattice constant of the $(CoFul)_\infty$ nanowire is determined to be 5.33 Å, while the calculated perpendicular Co-Cyclopentadiene distance is 1.71 Å. The H-C bond lengths are found to be 1.09 Å, and the C-C bond lengths range from 1.43 Å to 1.44 Å. We preliminarily evaluate the electronic stability of the $(CoFul)_\infty$ nanowire using the binding energy, defined as $E_b = E_w - E_{Co} - E_{Ful}$, where E_w, E_{Co} and E_{Ful} represent total energies of the nanowire, Co atom, and fulvalene molecule, respectively. The binding energy is calculated to be –6.1 eV, indicating good electronic stability. At room temperature of 300 K, the ab initio molecular dynamics (AIMD) simulations are performed to assess the thermodynamic stability of the $(CoFul)_\infty$ nanowire, and the phonon dispersion is also calculated to confirm the dynamic stability. As illustrated in Supplementary Figs. 1, 2, the results suggest that the structure is thermally and dynamically stable. Finally, we access the $(CoFul)_\infty$ nanowire's chemical stability through the adsorption of O_2, and the results show that the O_2 cannot be adsorbed (more details can be seen in Supplementary Figs. 3 and 4). The sheltering effect of the fulvalene renders the Co atom inert in the ambient air. These findings highlight the role of the fulvalene in stabilizing both the physical and chemical stabilities of the $(CoFul)_\infty$ nanowire.

Magnetic, electronic, and transport properties

Next, we investigate the magnetism and conductivity of the $(CoFul)_\infty$ nanowire. Similarly, the $(CoFul)_\infty$ also prefers the FM phase and a magnetic moment of 1 μ_B is predominantly localized at the Co atom (Fig. 2c). Since the axis orientation of the d_{z^2} orbital of Co is not aligned with the z-direction of the unit cell, the utilization of the conventional projected density of states (PDOS) analysis based on the coordinates of the unit cell, is inapplicable in this system. To decipher the orbital nature of the magnetic moment, we employ a more advanced analysis technique, namely the solid state adaptive natural density partitioning (SSAdNDP) (see Supplementary Fig. 5 for details)[57]. Our analysis reveals that the 1 μ_B magnetic moment is derived from the hybrid d_{yz} and d_{xz} orbital of Co with occupation numbers of 0.49 |e| and 0.48 |e|, respectively (Fig. 2d). The band structure of the $(CoFul)_\infty$ nanowire also corroborates this finding. As depicted in Fig. 2b, the $(CoFul)_\infty$

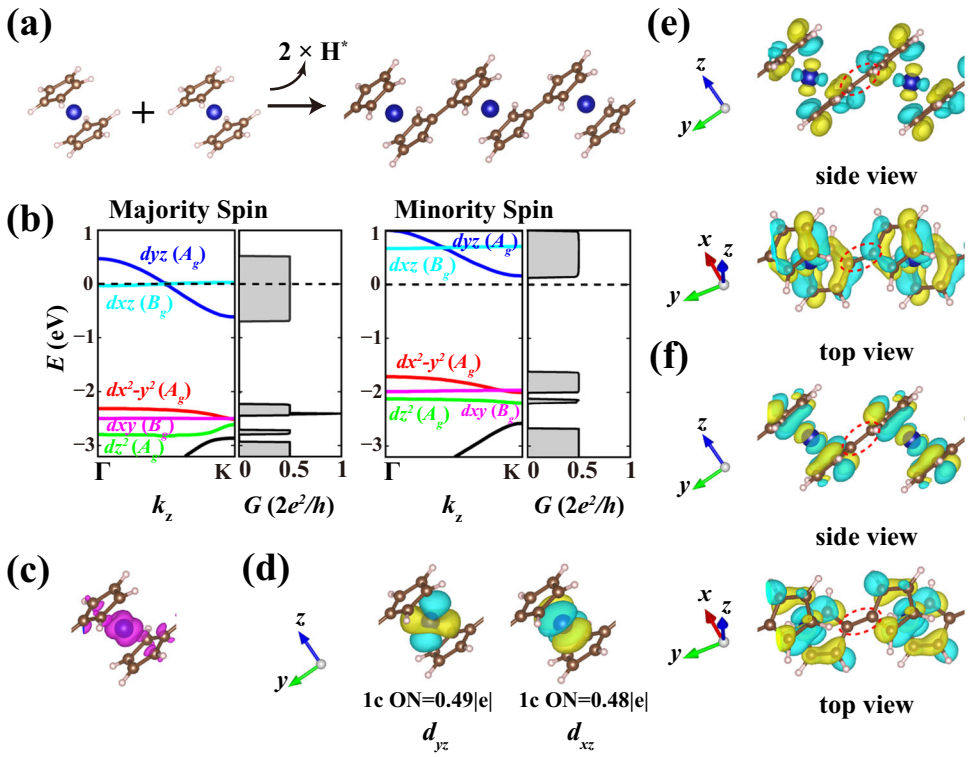

Fig. 2 The atomic structure and electronic, magnetic and transport properties of the $(CoFul)_\infty$ nanowire. a Schematic for the synthesis of the 1D $(CoFul)_\infty$ nanowire from the polymerization of Cobaltocene molecules. **b** The spin-polarized band structure, conductivity and **c** spin charge density isosurface of the $(CoFul)_\infty$ nanowire. **d** The Co lone pair hybrid bond (1c bond) consists of d_{yz} orbital with occupancy of 0.49 |e| and d_{xz} orbital with occupancy of 0.48 |e| responsible for the 1 μ_B magnetic moment in the $(CoFul)_\infty$ nanowire. **e** The side views and top views of the wavefunctions o**f** the d_{yz} band and **f** the d_{xz} band in the band structure shown in **b**.

exhibits half-metallicity, in which the majority spin channel is metallic while the minority spin channel shows an indirect band gap of 1.87 eV. Similar to the situation of Co nanowire, the bands near the Fermi level are also dominated by the *d* orbitals of Co. The behavior of the frontier bands near the Fermi level can be explained by crystal field theory combined with molecular orbital theory as follows. It's noteworthy that the principal symmetry axis of the $(CoFul)_\infty$ nanowire is along the *x*-axis, resulting in higher C_{2h} symmetry instead of the lower C_i symmetry when either *y*-axis or *z*-axis is considered as the principal axis. The d_{yz}, d_{z^2} and $d_{x^2-y^2}$ orbitals of Co exhibit symmetry with respect to C_2 operation, possessing A_g symmetry, while the d_{xz} and d_{xy} orbitals are antisymmetric and thus exhibit B_g symmetry. Under the C_{2h} crystal field, the *d* orbitals of Co experience energy level split due to their different coupling strengths with the π orbitals of the fulvalene. For instance, since the orbital lobes of d_{xy} and $d_{x^2-y^2}$ are parallel to the fulvalene plane (Supplementary Fig. 6), their overlap with the π orbitals of fulvalene is minimal, resulting in two localized d_{xy} and $d_{x^2-y^2}$ bands located far from the Fermi level in both the majority and the minority spin channels. The least overlap between d_{z^2} orbital and π orbital can be anticipated since the orbital lobes of d_{z^2} are pointed towards the "holes" of the carbocycles. Consequently, a localized d_{z^2} band is formed with an energy level lower than that of all other *d* bands. On the contrary, the remaining d_{yz} orbital and d_{xz} orbital of Co, vertically oriented toward the carbocycles, have appreciable coupling with the π orbitals of fulvalene (Fig. 2e, f), which give rise to two half-occupied bands at the Fermi level in the majority spin channel. The flat d_{xz} band, mainly composed of the localized Bloch states, makes little contribution to the conductivity in realistic electronic devices, as will be demonstrated later. Thus, only the dispersive d_{yz} band contributes a single-spin conductance channel, characterized by a conductance plateau of 0.5 G_0 around the Fermi level (Fig. 2b). In the minority spin channel, both the d_{yz} and d_{xz} bands are unoccupied, displaying a semiconductor behavior.

To elucidate why originally degenerate d_{yz} and d_{xz} bands in the Co nanowire (Fig. 1b) are split into a dispersive d_{yz} band and a flat d_{xz} band, respectively, in the $(CoFul)_\infty$ nanowire (Fig. 2b), we compare the wavefunctions of the d_{yz} and d_{xz} bands of the $(CoFul)_\infty$ nanowire (Fig. 2e, f) with the frontier molecular orbitals of fulvalene (Fig. 3a). Due to symmetry matching, only the LUMO (A_g symmetry) and HOMO-1 (B_g symmetry) of fulvalene exhibit nonzero overlap with the d_{yz} (A_g symmetry) and d_{xz} (B_g symmetry) orbitals of Co, respectively. The HOMO-1 of fulvalene is highly localized and no electron density resides on the exocyclic C-C double bond between the two five-membered rings (Fig. 3a). Thus, two adjacent Co atoms cannot interact with each other through the localized HOMO-1 of fulavelne (the top view of Fig. 2f), rendering a flat d_{xz} band at the Fermi level. The situation is opposite for the d_{yz} band because strong interaction between two adjacent Co atoms is facilitated through the diffused LUMO (the top view of Fig. 2e), yielding an open ballistic conductance channel. These findings demonstrate that the fulvalene acts as a mediator of the interaction between the Co atoms, and this mediation is orbital-selective: the majority of *d* orbitals are blocked, while only permitting the d_{yz} orbital to form the long-range interaction between the adjacent Co atoms.

To investigate the feasibility of achieving quantized half-integer conductance in realistic electronic devices, we have examined the transport properties of finite-sized $(CoFul)_n$ nanowires connected between two bulk Co(111) electrodes. The devices are constructed by connecting $(CoFul)_n$ nanowires of varying lengths ($(CoFul)_3$, $(CoFul)_5$, $(CoFul)_7$ and $(CoFul)_9$) to the hollow sites of the Co(111) surfaces, as depicted in Supplementary Fig. 7. The transport calculations demonstrate that as the length of the $(CoFul)_n$ nanowire increases, the conductance of the device rapidly

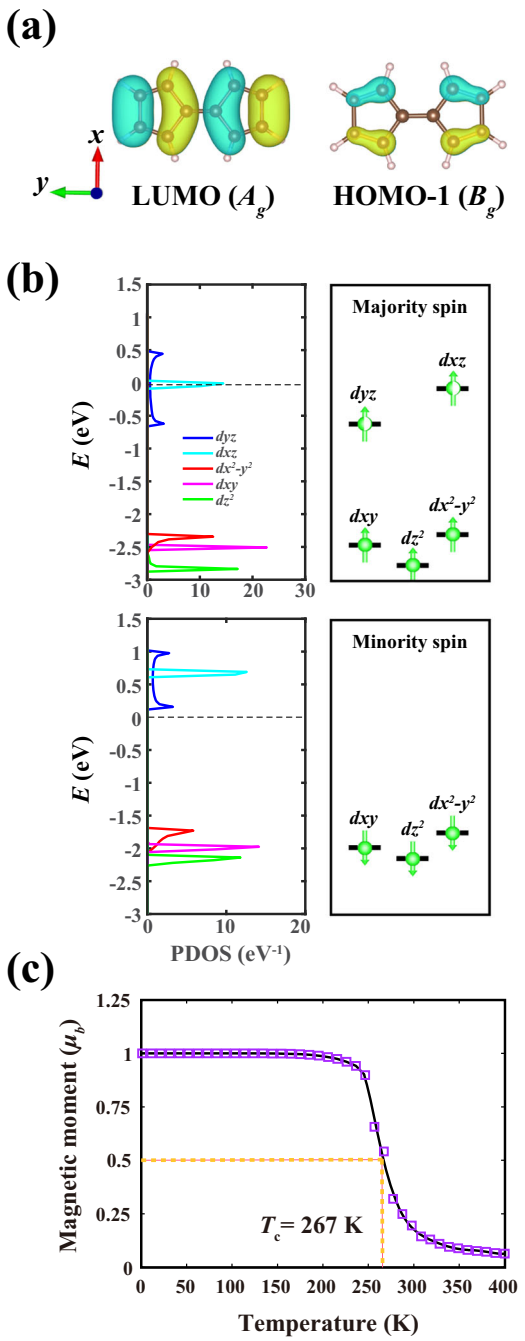

Fig. 3 The molecular orbitals of the fulvalene and the electron configuration and Curie temperature of the $(CoFul)_\infty$ nanowire. **a** The LUMO and HOMO-1 of the fulvalene. **b** The PDOS and the *d* orbital occupation diagram of Co in the $(CoFul)_\infty$ nanowire. The PDOS in the left panel is obtained from the band structure in Fig. 2b. The direction of the arrow in the right panel represents the majority spin or minority spin and the full-filled or half-filled ball represents full occupation or half occupation, respectively. **c** The variation of the total magnetic moment per unit cell of the 2D $(CoFul)_\infty$ nanowire array with respect to the temperature.

converges to 0.5 G_0 (Supplementary Fig. 8a), and the $(CoFul)_7$ nanowire is sufficiently long to exhibit half-integer conductance. To unravel the underlying transport mechanism responsible for the observed half-integer conductance, we have calculated the tunneling eigenchannel of the $(CoFul)_7$ device. As shown in Supplementary Fig. 8b, the tunneling eigenchannel consists of only the d_{yz} orbitals of Co and the dispersive π orbitals of fulvalenes, which is consistent with the conduction mechanisms of 1D infinite $(CoFul)_\infty$ nanowire.

Origin of magnetic moment and half-metallicity

We have proposed a simplified schematic model to elucidate the origin of the magnetic moment and half-metallicity in the $(CoFul)_\infty$ nanowire. The *d* orbital occupation diagram of Co is constructed based on the PDOS of Co in the $(CoFul)_\infty$ nanowire. As illustrated in Fig. 3b, the energy level of each *d* orbital in the right panel is aligned with the peak position of corresponding *d* orbital in the PDOS in the left panel. The occupation of each *d* orbital is determined by integrating the PDOS of the corresponding *d* orbital below the Fermi level. The Co possesses nine valence electrons ($3d^7 4s^2$), and according to the Hückel rule, two electrons will be captured by the fulvalene to form a stable aromatic configuration of $4m + 2$ electrons. Six other electrons occupy the $d_{x^2-y^2}$, d_{xy}, and d_{z^2} orbitals in both the majority and minority spin channels (Fig. 3b). Lastly, the remaining one electron will half-occupy the degenerate d_{yz} and d_{xz} orbitals, respectively, in the majority spin channel, which is responsible for the magnetic moment of 1 μ_B and the appearance of half-metallicity. On the other hand, the degenerate d_{yz} and d_{xz} orbitals in the minority spin channel are unoccupied, leading to the semiconducting characteristic.

For comparison, we have also performed calculations using the PBE + U scheme[58]. The Hubbard parameter $U_{\text{eff}} = U\text{-}J$ is set to 3.3 eV for Co, which has been widely used in previous reports[59–62]. The results demonstrate that the main signatures, including the half-integer conductance and FM ground state with a magnetic moment of 1 μ_B, are still preserved. In comparison with the results of PBE functional, the differences are a widened band gap of the minority spin channel from 1.87 eV to 3.24 eV (Supplementary Fig. 9) and a slight increase of ΔE_{ex} from 0.103 eV to 0.112 eV.

In order to gain further insights of the magnetic interactions, we have also investigated the exchange couplings of the $(CoFul)_\infty$ nanowire. The exchange coupling of the $(CoFul)_\infty$ nanowire was studied using the Ising model $H = -\sum_{\langle i,j\rangle} JS_iS_j - \sum_{\langle\langle i,j\rangle\rangle} J'S_iS_j$, where J and J' represent the exchange couplings for the nearest-neighbor and next nearest-neighbor sites, respectively, and S_i denotes the magnetic moment at each site. To obtain the exchange couplings, we have considered three magnetic configurations: FM, AFM1 and AFM2 in a $(1 \times 1 \times 4)$ supercell, as displayed in the Supplementary Fig. 10. By mapping the total energies obtained by PBE + U scheme to the Ising spin Hamiltonian, the exchange couplings can be determined,

$$E_{\text{FM}} = E_0 - 4J|S|^2 - 4J'|S|^2 \quad (1)$$

$$E_{\text{AFM1}} = E_0 + 4J|S|^2 - 4J'|S|^2 \quad (2)$$

$$E_{\text{AFM2}} = E_0 + 4J'|S|^2 \quad (3)$$

where E_0 is the ground state energy independent of the spin configuration and S is the spin on each Co atom. The calculated values of J and J' are 28 meV and 4.2 meV, respectively, for the $(CoFul)_\infty$ nanowire. Clearly, the nearest-neighbor exchange coupling dominates in the $(CoFul)_\infty$ nanowire. Similarly, applying the same procedure, the J and J' of the Co nanowire are estimated to be 32.4 meV and 8.1 meV, respectively.

Notably, the possibility of Peierls transition needs to be assessed since if a partially filled band crosses the Fermi level exactly at the wavevector $k = \pi/2c$ (c is the lattice constant), a structural distortion of dimerization may happen because of the strong electron-phonon interaction[63]. In this case, we duplicate the unit cell and optimize lattice of the supercell structure. Actually, no dimerization occurs, revealing that the coupling between the Co and the fulvalene is strong enough to prevent the Peierls transition.

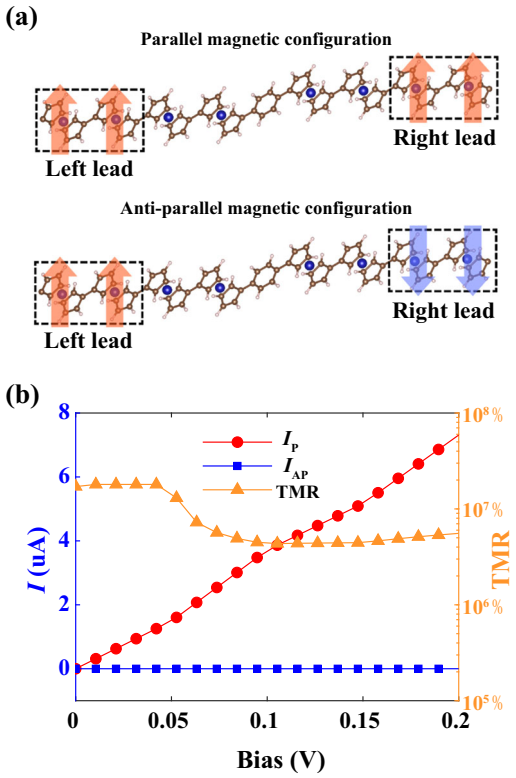

Fig. 4 The atomic structure and transport properties of the $(CoFul)_\infty$-benzene-$(CoFul)_\infty$ device. a The schematic structures of the $(CoFul)_\infty$-benzene-$(CoFul)_\infty$ device in parallel and anti-parallel magnetic configurations. **b** The *I*–*V* curves of the $(CoFul)_\infty$-benzene-$(CoFul)_\infty$ device in parallel and anti-parallel magnetic configurations (left vertical axis) and the derived TMR ratio (right vertical axis).

It is worth noting that a recent wonderful theoretical work has also reported a half-metallic nanowire, $(CoH_3)_\infty$[21], capable of producing 100% spin-polarized current. In that system, the bands crossing the Fermi level in the majority spin channel are two-fold degenerate d_{xy} and $d_{x^2-y^2}$ bands, contributing two ballistic conductance channels instead of single ballistic channel.

Finally, we have also investigated the electronic and magnetic properties of a class of $(TMFul)_\infty$ nanowires constructed by substituting the metal atom with all other 3*d*-block transition metals. As summarized in Supplementary Table 1, the $(TMFul)_\infty$ nanowires display diverse electrical and magnetic properties. Among them, $(ScFul)_\infty$, $(TiFul)_\infty$, $(MnFul)_\infty$ and $(NiFul)_\infty$ favor the AFM ground states, while $(VFul)_\infty$ and $(CrFul)_\infty$ prefer the FM ground state. The $(FeFul)_\infty$ is non-magnetic (NM) with a largest band gap of 2.96 eV. Interestingly, the band gap values span evenly between 0 and 3 eV. Thanks to their diverse characteristics, this class of $(TMFul)_\infty$ nanowires have great prospects in a wide range of applications, including transistors, optoelectronics and magnetic memory devices. Although this category of $(TMFul)_\infty$ nanowires present diverse characteristics, in this work, we pay particular attention to the $(CoFul)_\infty$ nanowire that displays half-integer conductance quantization.

Curie temperature and spintronic device performance

To develop practical spintronics with the $(CoFul)_\infty$ nanowire, understanding the variation of magnetic moment with regard to temperature is crucial. Despite the Mermin-Wagner theorem[64] suggesting that long-range magnetic ordering is unlikely in an infinite 1D chain at nonzero temperature, many studies have demonstrated that the magnetic ordering can be stabilized in a stacking nanowire bundle or a 2D nanowire array, where the interchain coupling plays a key role in this behavior[65–68]. For instance, an experimental study showed that a weak interchain coupling of 0.1 K (0.009 meV) was strong enough to establish long-range Ferromagnetic ordering in quasi-1D p-NPNN nanowire[65]. On the basis of this discovery, we build a 2D $(CoFul)_\infty$ nanowire array and then perform a Monte Carlo (MC) simulation[69,70] to determine its Curie temperature (T_c) based on the Ising model $H = -\sum_{\langle i,j \rangle} JS_iS_j$, where J is the nearest-neighbor exchange parameter. The optimal interchain distance of the 2D $(CoFul)_\infty$ nanowire array is determined from the curve of the total energy versus interchain distance. For each fixed interchain distance, we optimized the structure using the DFT + D3 scheme[71] to include the van der Waals interactions, and then obtained the total energy after the optimization. The results are shown in Supplementary Fig. 11, and the optimal interchain distance is estimated to be 6.5 Å. The intrachain exchange coupling J_1 and the interchain exchange coupling J_2 of the 2D nanowire array (Supplementary Fig. 12) are calculated to be 28 meV and 2.1 meV, respectively, by PBE + U scheme. In the MC simulation, we use a (100 × 100) supercell and perform 1×10^9 loops to achieve the average magnetic moment for each temperature value. The temperature dependence of the average magnetic moment per unit cell is shown in Fig. 3c, with an estimated T_c of 267 K. This value is significantly higher than that of quasi-1D $CrSbSe_3$ nanowire (95 K)[68].

The characteristics of the $(CoFul)_\infty$ nanowire offer exciting opportunities for spintronic applications. Here, we exemplarily showcase how well it performs as a spin filter or spin valve device. As illustrated in Fig. 4a, a molecular magnetic tunneling junction (MTJ)[31] is constructed by coupling benzene between two $(CoFul)_\infty$ nanowire electrodes. The structure of the entire molecular junction has been optimized and the results show that the benzene favors a coplanar configuration with the cyclopentadiene cycles (Supplementary Fig. 13). The spin-filter efficiency (SFE) and tunneling magneto-resistance (TMR) of the device are assessed using the following formulas:

$$\mathrm{SFE} = \frac{(I_\uparrow - I_\downarrow)}{(I_\uparrow + I_\downarrow)} \times 100\% \tag{4}$$

$$\mathrm{TMR} = \frac{(I_P - I_{AP})}{I_{AP}} \times 100\% \tag{5}$$

where the $I_\uparrow$ and $I_\downarrow$ are majority spin and minority spin currents, respectively, and the I_P and I_{AP} are the currents in parallel and anti-parallel magnetic configurations, respectively. Our spin transport simulations show that the SFE is nearly 100% even when the current reaches up to 7 μA (Supplementary Fig. 14). Additionally, a staggering TMR of ~10^7% is recorded throughout the whole bias range, which, to the best of our knowledge, represents the best record in the field of molecular MTJs to date. (Fig. 4b). In this device, a huge TMR can be achieved without compromising the current's strength. It has addressed a critical limitation observed in many previously reported organic-semiconductor-based MTJs[72], namely, an extremely low on-state current is produced in order to achieve a huge TMR, which is detrimental to real device operation. These findings show that the $(CoFul)_\infty$ nanowire can function flawlessly as a spin filter or spin valve device. For comparison, the TMRs of other 3D, 2D, and 1D molecular MTJ systems are as follows: bulk Ni (600%)[31], bulk Co (60%)[73], 2D Fe_3GeTe_2 (6×10^3%)[74], Co nanowire (2×10^4%)[75], $(CoCp_2)_\infty$ nanowire (25%)[76] and Fe_3O_4 nanowire (2×10^4%)[77]. Notably, Kim et al. theoretically predicted that quasi-1D graphene nanoribbon (GNR) would exhibit an amazing TMR of 10^6%[78,79]. However, the GNR still confronts challenges for practical application because experimental works have demonstrated that the graphene exhibits no signs of ferromagnetism at any temperature[80,81]. The absence of ferromagnetic behavior is ascribed to weak ferromagnetic exchange coupling among the magnetic moments in carbon-based materials[82,83].

The giant TMR observed in the $(CoFul)_\infty$-based MTJ is primarily attributed to the characteristic of single-spin channel transport in the $(CoFul)_\infty$ electrodes. Generally, the transport in an MTJ is dominated by two key factors, namely, the coupling between the molecule and electrodes, and the matching of Bloch states between two electrodes. For the parallel magnetic configuration, the transport is dominated by the coupling between the molecule and electrodes because the Bloch states in two electrodes are already well matched. According to the tunneling eigenchannel analysis (Supplementary Fig. 15b)[84], the LUMO of benzene can strongly couple with the Bloch states of the d_{yz} bands in the electrodes, resulting in a conductance of 0.49 G_0 at the Fermi level for the majority spin (Supplementary Fig. 15a). Considering the fact that the benzene is connected to the electrodes through the C-C single bonds, the conductance limit of this MTJ is restricted strictly to 0.5 G_0 for either majority spin or minority spin, regardless of how many spin channels are available for transport in the electrodes. In other words, the conductance of this MTJ in the parallel magnetic configuration has already been maximized with the help of the strong coupling between the LUMO of benzene and the d_{yz} bands of electrodes. In contrast, the transport in the anti-parallel magnetic configuration is dominated by the mismatch of Bloch states between two electrodes. Since only single-spin channel is available for transport in the electrodes, combined with a large energy mismatch between the d_{yz} band of the majority spin in the left electrode and the d_{yz} band of the minority spin in the right electrode, the conductance of this MTJ is minimized to a mere 2.8×10^{-6} G_0 (Supplementary Fig. 15c). Evidently, the d_{yz} band serves opposing roles in the parallel and anti-parallel magnetic configurations: it maximizes the transport in the parallel magnetic configuration through strong coupling with the LUMO of benzene while simultaneously minimizing the transport in the anti-parallel magnetic configuration via a large mismatch between the d_{yz} bands of two electrodes. This mechanism results in a staggering TMR observed in this molecular MTJ.

DISCUSSION

In conclusion, using the first-principles methods, we have investigated the electronic, magnetic, and transport properties of the $(CoFul)_\infty$ nanowire. The $(CoFul)_\infty$ nanowire is a half-metallic ferromagnet that exhibits single-spin channel transport characteristics, and its magnetic moment arises from the half-occupied d_{yz} and d_{xz} orbitals of the Co atom. By comparing with a pure Co nanowire, we have demonstrated that the incorporation of fulvalene has three-fold effects in the $(CoFul)_\infty$ nanowire: (1) stabilization of the structure and reduction of environmental contamination; (2) establishment of a single ballistic conductance channel by splitting the two-fold degenerate d_{yz} and d_{xz} bands and blocking one of these two conductance channels; (3) maintaining the superexchange coupling between adjacent Co atoms. Furthermore, a class of $(TMFul)_\infty$ nanowires exhibit an abundance of desirable properties, making them attractive candidates for multifunctional spintronics. In this work, we particularly focus on the spintronic device performance of the $(CoFul)_\infty$ nanowire. Benefiting from the spin transmitting confined in a single open spin channel, the $(CoFul)_\infty$-based molecular MTJ can function flawlessly as a spin filter or spin valve device.

METHODS

First-principles calculations details

All first-principles calculations based on the spin-polarized density functional theory (DFT) were carried out by using the Vienna ab Initio Simlation Package (VASP)[85,86]. The Projector augmented wave pseudopotentials[87] for the core and the Perdew-Burke-Ernzerhof (PBE) format[88] of the generalized gradient approximation (GGA) for the exchange-correlation functional were adopted. The DFT-D3 scheme[71] was used to account for the van der Waals interaction. We set the kinetic energy cutoff to be 520 eV, and optimized the structures until the forces were below 0.01 eV/Å. To eliminate the interaction between the nanowire and its images, the vacuum spaces in the x and y directions were set to be 20 Å. The Brillouin Zones of the Co nanowire and the $(CoFul)_\infty$ nanowire were sampled by $1 \times 1 \times 23$ and $1 \times 1 \times 9$ k points, respectively, in the Monkhorst-Pack scheme. In order to assess the thermal dynamic stability, AIMD simulations were performed in the canonical ensemble with Nosé-Hoover thermostat (NVT). In the AIMD simulations, a $(1 \times 1 \times 2)$ supercell was used and each time-step of 1 fs was adopted for a total duration of 2 ps at 300 K. For the analysis of the chemical bonding pattern in the $(CoFul)_\infty$ nanowire, we used the SSAdNDP scheme[57] by projecting the delocalized plane-wave basis set from the VASP code to a localized Karlsruhe def2-SVP basis set.

Transport properties calculations details

All the transport calculations were performed with the steady-state (SS)-DFT[89–92]. In the transport simulations, Troullier-Martins pseudopotentials[93] for the core and double-ζ polarized (DZP) basis set were employed. The tunneling eigenchannel analysis was done by the software INELASTICA[94].

DATA AVAILABILITY

All the data supporting the results of this study are available within the main manuscript and the Supplementary Information. Additional data related to this study are available from the corresponding authors upon reasonable request.

CODE AVAILABILITY

The relevant codes are available from the corresponding authors upon reasonable request.

Received: 23 March 2023; Accepted: 4 October 2023;
Published online: 21 October 2023

REFERENCES

1. Gambardella, P. et al. Ferromagnetism in one-dimensional monatomic metal chains. *Nature* **416**, 301–304 (2002).
2. Rodrigues, V., Bettini, J., Silva, P. C. & Ugarte, D. Evidence for spontaneous spin-polarized transport in magnetic nanowires. *Phys. Rev. Lett.* **91**, 096801 (2003).
3. Miyajima, K., Nakajima, A., Yabushita, S., Knickelbein, M. B. & Kaya, K. Ferromagnetism in one-dimensional vanadium-benzene sandwich clusters. *J. Am. Chem. Soc.* **126**, 13202–13203 (2004).
4. Bettini, J. et al. Experimental realization of suspended atomic chains composed of different atomic species. *Nat. Nanotechnol.* **1**, 182–185 (2006).
5. Crook, R. et al. Conductance quantization at a half-integer plateau in a symmetric GaAs quantum wire. *Science* **312**, 1359–1362 (2006).
6. Maslyuk, V. V. et al. Organometallic benzene-vanadium wire: a one-dimensional half-metallic ferromagnet. *Phys. Rev. Lett.* **97**, 097201 (2006).
7. Xiang, H. J., Yang, J. L., Hou, J. G. & Zhu, Q. S. One-dimensional transition metal-benzene sandwich polymers: Possible ideal conductors for spin transport. *J. Am. Chem. Soc.* **128**, 2310–2314 (2006).
8. Sokolov, A., Zhang, C., Tsymbal, E. Y., Redepenning, J. & Doudin, B. Quantized magnetoresistance in atomic-size contacts. *Nat. Nanotechnol.* **2**, 171–175 (2007).
9. Shen, L. et al. Charge-transfer-based mechanism for half-metallicity and ferromagnetism in one-dimensional organometallic sandwich molecular wires. *J. Am. Chem. Soc.* **130**, 13956–13960 (2008).
10. Wang, L. et al. Novel one-dimensional organometallic half metals: vanadium-cyclopentadienyl, vanadium-cyclopentadienyl-benzene, and vanadium-anthracene wires. *Nano Lett.* **8**, 3640–3644 (2008).
11. Thiess, A., Mokrousov, Y., Heinze, S. & Blugel, S. Magnetically hindered chain formation in transition-metal break junctions. *Phys. Rev. Lett.* **103**, 217201 (2009).
12. Wu, X. J. & Zeng, X. C. Double metallocene nanowires. *J. Am. Chem. Soc.* **131**, 14246–14248 (2009).
13. Zhang, X. Y., Ng, M. F., Wang, Y. B., Wang, J. L. & Yang, S. W. Theoretical studies on structural, magnetic, and spintronic characteristics of sandwiched EunCOTn+1 (n=1-4) Clusters. *ACS Nano* **3**, 2515–2522 (2009).

14. Zhang, X. Y., Wang, J. L., Gao, Y. & Zeng, X. C. Ab initio study of structural and magnetic properties of TMn(ferrocene)(n+1) (TM = Sc, Ti, V, Mn) sandwich clusters and nanowires (n = infinity). *ACS Nano* **3**, 537–545 (2009).
15. Quay, C. H. L. et al. Observation of a one-dimensional spin–orbit gap in a quantum wire. *Nat. Phys.* **6**, 336–339 (2010).
16. Zhang, Z. H., Wu, X. J., Guo, W. L. & Zeng, X. C. Carrier-tunable magnetic ordering in vanadium-naphthalene sandwich nanowires. *J. Am. Chem. Soc.* **132**, 10215–10217 (2010).
17. Wu, M., Burton, J. D., Tsymbal, E. Y., Zeng, X. C. & Jena, P. Multiferroic materials based on organic transition-metal molecular nanowires. *J. Am. Chem. Soc.* **134**, 14423–14429 (2012).
18. Hsu, B. B. et al. The density of states and the transport effective mass in a highly oriented semiconducting polymer: electronic delocalization in 1D. *Adv. Mater.* **27**, 7759–7765 (2015).
19. Du, Y. et al. One-dimensional van der Waals material tellurium: raman spectroscopy under strain and magneto-transport. *Nano Lett.* **17**, 3965–3973 (2017).
20. Huttmann, F., Schleheck, N., Atodiresei, N. & Michely, T. On-surface synthesis of sandwich molecular nanowires on graphene. *J. Am. Chem. Soc.* **139**, 9895–9900 (2017).
21. Li, X. L. et al. Half-metallicity in one-dimensional metal trihydride molecular nanowires. *J. Am. Chem. Soc.* **139**, 6290–6293 (2017).
22. Liang, Q., Chang, X., Su, Y. Q., Mugo, S. M. & Zhang, Q. Mechanistic investigation on copper-arylacetylide polymerization and sensing applications. *Angew. Chem. Int. Ed.* **60**, 18014–18021 (2021).
23. Mallada, B. et al. On-Surface Synthesis of One-Dimensional Coordination Polymers with Tailored Magnetic Anisotropy. *ACS Appl. Mater. Interfaces* **13**, 32393–32401 (2021).
24. Ohnishi, H., Kondo, Y. & Takayanagi, K. Quantized conductance through individual rows of suspended gold atoms. *Nature* **395**, 780–783 (1998).
25. Rodrigues, V., Bettini, J., Rocha, A. R., Rego, L. G. C. & Ugarte, D. Quantum conductance in silver nanowires: Correlation between atomic structure and transport properties. *Phys. Rev. B* **65**, 153402 (2002).
26. Li, C. Z. & Tao, N. J. Quantum transport in metallic nanowires fabricated by electrochemical deposition/dissolution. *Appl. Phys. Lett.* **72**, 894–896 (1998).
27. Lehmann, J., Gaita-Ariño, A., Coronado, E. & Loss, D. Spin qubits with electrically gated polyoxometalate molecules. *Nat. Nanotechnol.* **2**, 312–317 (2007).
28. Graham, A. C. et al. Interaction effects at crossings of spin-polarized one-dimensional subbands. *Phys. Rev. Lett.* **91**, 136404 (2003).
29. Tang, J. et al. Ferromagnetic germanide in Ge nanowire transistors for spintronics application. *ACS Nano* **6**, 5710–5717 (2012).
30. Smogunov, A. & Dappe, Y. J. Symmetry-derived half-metallicity in atomic and molecular junctions. *Nano Lett.* **15**, 3552–3556 (2015).
31. Rocha, A. R. et al. Towards molecular spintronics. *Nat. Mater.* **4**, 335–339 (2005).
32. Cespedes, O., Wheeler, M., Moorsom, T. & Viret, M. Unexpected magnetic properties of gas-stabilized platinum nanostructures in the tunneling regime. *Nano Lett.* **15**, 45–50 (2015).
33. Jia, C., Lin, Z., Huang, Y. & Duan, X. Nanowire electronics: from nanoscale to macroscale. *Chem. Rev.* **119**, 9074–9135 (2019).
34. Hong, J. & Wu, R. Q. First principles calculations of magnetic anisotropy energy of Co monatomic wires. *Phys. Rev. B* **67**, 020406 (2003).
35. Nautiyal, T., Rho, T. H. & Kim, K. S. Nanowires for spintronics: a study of transition-metal elements of groups 8–10. *Phys. Rev. B* **69**, 193404 (2004).
36. Smogunov, A., Dal Corso, A. & Tosatti, E. Ballistic conductance of magnetic Co and Ni nanowires with ultrasoft pseudopotentials. *Phys. Rev. B* **70**, 045417 (2004).
37. Untiedt, C., Dekker, D. M. T., Djukic, D. & van Ruitenbeek, J. M. Absence of magnetically induced fractional quantization in atomic contacts. *Phys. Rev. B* **69**, 081401 (2004).
38. Sabirianov, R. F., Solanki, A. K., Burton, J. D., Jaswal, S. S. & Tsymbal, E. Y. Domain-wall magnetoresistance of Co nanowires. *Phys. Rev. B* **72**, 054443 (2005).
39. Wierzbowska, M., Delin, A. & Tosatti, E. Effect of electron correlations in Pd, Ni, and Co monowires. *Phys. Rev. B* **72**, 035439 (2005).
40. Ke et al. conductance calculation of atomic-scale nanowires of Au and Co. *Nanotechnology* **18**, 095709 (2007).
41. Tung, J. C. & Guo, G. Y. Systematicab initiostudy of the magnetic and electronic properties of all3dtransition metal linear and zigzag nanowires. *Phys. Rev. B* **76**, 094413 (2007).
42. Häfner, M. et al. Theoretical study of the conductance of ferromagnetic atomic-sized contacts. *Phys. Rev. B* **77**, 104409 (2008).
43. Hope, B. & Horsfield, A. Contrasting spin-polarization regimes in Co nanowires studied by density functional theory. *Phys. Rev. B* **77**, 094442 (2008).
44. Vardimon, R., Matt, M., Nielaba, P., Cuevas, J. C. & Tal, O. Orbital origin of the electrical conduction in ferromagnetic atomic-size contacts: insights from shot noise measurements and theoretical simulations. *Phys. Rev. B* **93**, 085439 (2016).
45. Thomas, K. J. et al. Possible spin polarization in a one-dimensional electron gas. *Phys. Rev. Lett.* **77**, 135–138 (1996).
46. Fisher, D. S. Random transverse field Ising spin chains. *Phys. Rev. Lett.* **69**, 534–537 (1992).
47. Bose, S. Quantum communication through an unmodulated spin chain. *Phys. Rev. Lett.* **91**, 207901 (2003).
48. Chen, X. et al. Probing superexchange interaction in molecular magnets by spin-flip spectroscopy and microscopy. *Phys. Rev. Lett.* **101**, 197208 (2008).
49. Fernández-Rossier, J. Theory of single-spin inelastic tunneling spectroscopy. *Phys. Rev. Lett.* **102**, 256802 (2009).
50. Goff, J. P., Tennant, D. A. & Nagler, S. E. Exchange mixing and soliton dynamics in the quantum spin chain $CsCoCl_3$. *Phys. Rev. B* **52**, 15992–16000 (1995).
51. Coldea, R. et al. Quantum criticality in an ising chain: experimental evidence for emergent E8 symmetry. *Science* **327**, 177–180 (2010).
52. Liu, F. et al. Confined quasiparticle dynamics in long-range interacting quantum spin chains. *Phys. Rev. Lett.* **122**, 150601 (2019).
53. Katoh, K. et al. Control of the spin dynamics of single-molecule magnets by using a quasi one-dimensional arrangement. *Angew. Chem. Int. Ed.* **57**, 9262–9267 (2018).
54. Sargolzaei, M. & Samaneh Ataee, S. First principles study on spin and orbital magnetism of 3d transition metal monatomic nanowires (Mn, Fe and Co). *J. Condens. Matter Phys.* **23**, 125301 (2011).
55. Barlow, S. & O'Hare, D. Metal−metal interactions in linked metallocenes. *Chem. Rev.* **97**, 637–670 (1997).
56. Inkpen, M. S. et al. Oligomeric ferrocene rings. *Nat. Chem.* **8**, 825–830 (2016).
57. Galeev, T. R., Dunnington, B. D., Schmidt, J. R. & Boldyrev, A. I. Solid state adaptive natural density partitioning: a tool for deciphering multi-center bonding in periodic systems. *Phys. Chem. Chem. Phys.* **15**, 5022–5029 (2013).
58. Dudarev, S. L., Botton, G. A., Savrasov, S. Y., Humphreys, C. J. & Sutton, A. P. Electron-energy-loss spectra and the structural stability of nickel oxide: an LSDA +U study. *Phys. Rev. B* **57**, 1505–1509 (1998).
59. Aykol, M. & Wolverton, C. Local environment dependent GGA+U method for accurate thermochemistry of transition metal compounds. *Phys. Rev. B* **90**, 115105 (2014).
60. Jain, A. et al. Formation enthalpies by mixing GGA and GGA+U calculations. *Phys. Rev. B* **84**, 045115 (2011).
61. Wang, L., Maxisch, T. & Ceder, G. Oxidation energies of transition metal oxides within the GGA+U framework. *Phys. Rev. B* **73**, 195107 (2006).
62. Aykol, M., Kim, S. & Wolverton, C. van der Waals interactions in layered lithium cobalt oxides. *J. Phys. Chem. C* **119**, 19053–19058 (2015).
63. Claessen, R. et al. Spectroscopic signatures of spin-charge separation in the quasi-one-dimensional organic conductor TTF-TCNQ. *Phys. Rev. Lett.* **88**, 096402 (2002).
64. Mermin, N. D. & Wagner, H. Absence of ferromagnetism or antiferromagnetism in one- or two-dimensional isotropic Heisenberg models. *Phys. Rev. Lett.* **17**, 1133–1136 (1966).
65. Takahashi, M. et al. Discovery of a quasi-1D organic ferromagnet, p-NPNN. *Phys. Rev. Lett.* **67**, 746–748 (1991).
66. Xiang, H., Yang, J., Hou, J. G. & Zhu, Q. One-dimensional transition metal−benzene sandwich polymers: possible ideal conductors for spin transport. *J. Am. Chem. Soc.* **128**, 2310–2314 (2006).
67. Friedlander, S. et al. Linear chains of magnetic ions stacked with variable distance: ferromagnetic ordering with a Curie temperature above 20 K. *Angew. Chem. Int. Ed.* **55**, 12683–12687 (2016).
68. Qu, Y., Arguilla, M. Q., Zhang, Q., He, X. & Dinca, M. Ultrathin, high-aspect ratio, and free-standing magnetic nanowires by exfoliation of ferromagnetic quasi-one-dimensional van der Waals lattices. *J. Am. Chem. Soc.* **143**, 19551–19558 (2021).
69. Binder K., Ceperley D. M. *Monte Carlo Methods in Statistical Physics*. (Springer-Verlag, 1986).
70. Liu, L. et al. Magnetic switches via electric field in BN nanoribbons. *Appl. Surf. Sci.* **480**, 300–307 (2019).
71. Grimme, S., Antony, J., Ehrlich, S. & Krieg, H. A consistent and accurate ab initio parametrization of density functional dispersion correction (DFT-D) for the 94 elements H-Pu. *J. Chem. Phys.* **132**, 154104 (2010).
72. Sanvito, S. Molecular spintronics. *Chem. Soc. Rev.* **40**, 3336–3355 (2011).
73. Schmaus, S. et al. Giant magnetoresistance through a single molecule. *Nat. Nanotechnol.* **6**, 185–189 (2011).
74. Li, D., Frauenheim, T. & He, J. Robust giant magnetoresistance in 2D Van der Waals molecular magnetic tunnel junctions. *ACS Appl. Mater. Interfaces* **13**, 36098–36105 (2021).
75. Yang, J.-F., Zhou, L., Han, Q. & Wang, X.-F. Bias-controlled giant magnetoresistance through cyclopentadienyl–iron multidecker molecules. *J. Phys. Chem. C* **116**, 19996–20001 (2012).
76. García-Suárez, V. M., Ferrer, J. & Lambert, C. J. Tuning the electrical conductivity of nanotube-encapsulated metallocene wires. *Phys. Rev. Lett.* **96**, 106804 (2006).
77. Sun, M., Wang, X. & Mi, W. Large magnetoresistance in Fe3O4/4,4′-bipyridine/Fe3O4 organic magnetic tunnel junctions. *J. Phys. Chem. C* **122**, 3115–3122 (2018).

78. Kim, W. Y. & Kim, K. S. Prediction of very large values of magnetoresistance in a graphene nanoribbon device. *Nat. Nanotechnol.* **3**, 408–412 (2008).
79. Zeng, M. G., Shen, L., Cai, Y. Q., Sha, Z. D. & Feng, Y. P. Perfect spin-filter and spin-valve in carbon atomic chains. *Appl. Phys. Lett.* **96**, 042104 (2010).
80. Sepioni, M. et al. Limits on Intrinsic Magnetism in Graphene. *Phys. Rev. Lett.* **105**, 207205 (2010).
81. Nair, R. R. et al. Spin-half paramagnetism in graphene induced by point defects. *Nat. Phys.* **8**, 199–202 (2012).
82. Červenka, J., Katsnelson, M. I. & Flipse, C. F. J. Room-temperature ferromagnetism in graphite driven by two-dimensional networks of point defects. *Nat. Phys.* **5**, 840–844 (2009).
83. Lee, H., Lee, H.-J. & Kim, S. Y. Room-temperature ferromagnetism from an array of asymmetric zigzag-edge nanoribbons in a graphene junction. *Carbon* **127**, 57–63 (2018).
84. Paulsson, M. & Brandbyge, M. Transmission eigenchannels from nonequilibrium Green's functions. *Phys. Rev. B* **76**, 115117 (2007).
85. Kresse, G. & Hafner, J. Ab initio molecular dynamics for liquid metals. *Phys. Rev. B* **47**, 558–561 (1993).
86. Kresse, G. & Furthmüller, J. Efficient iterative schemes for ab initio total-energy calculations using a plane-wave basis set. *Phys. Rev. B* **54**, 11169–11186 (1996).
87. Blöchl, P. E. Projector augmented-wave method. *Phys. Rev. B* **50**, 17953–17979 (1994).
88. Perdew, J. P., Burke, K. & Ernzerhof, M. Generalized gradient approximation made simple. *Phys. Rev. Lett.* **77**, 3865–3868 (1996).
89. Liu, S., Nurbawono, A. & Zhang, C. Density functional theory for steady-state nonequilibrium molecular junctions. *Sci. Rep.* **5**, 15386 (2015).
90. Liu, S. L., Xi, Y. J., Guo, N., Yam, K. M. & Zhang, C. Spin-dependent electron transport through a Mn-phthalocyanine molecule-a steady-state density functional theory (SS-DFT) study. *Can. J. Chem.* **94**, 1002–1005 (2016).
91. Jiang, Z. et al. Prominent nonequilibrium effects beyond the standard first-principles approach in nanoscale electronic devices. *Nanoscale Horiz* **6**, 801–808 (2021).
92. Liu, S., Feng, Y. P. & Zhang, C. Communication: electronic and transport properties of molecular junctions under a finite bias: A dual mean field approach. *J. Chem. Phys.* **139**, 191103 (2013).
93. Troullier, N. & Martins, J. L. Efficient pseudopotentials for plane-wave calculations. *Phys. Rev. B* **43**, 1993–2006 (1991).
94. Frederiksen, T., Paulsson, M., Brandbyge, M. & Jauho, A.-P. Inelastic transport theory from first principles: Methodology and application to nanoscale devices. *Phys. Rev. B* **75**, 205413 (2007).

ACKNOWLEDGEMENTS

Y.S.A. is supported by the Singapore Ministry of Education (MOE) Academic Research Fund (ArRF) Tier 2 Grant (MOE-T2EP50221-0019) and the SUTD Kickstarter Initiatives (SKI) under the Award No. SKI 2021_01_12. C.Z. acknowledges the support of the Singapore Ministry of Education (MOE) Academic Research Fund (MOE2019-T2-2-030).

AUTHOR CONTRIBUTIONS

C.Z. and Y.S.A. conceived the project. Z.L.J. and K.M.Y. did all the calculations and contributed equally to this work. Z.L.J. and Y.S.A. provided the first draft. C.Z. and Y.S.A. revised the paper. All contributed to data analysis and finalization of the paper.

COMPETING INTERESTS

The authors declare no competing interests.

ADDITIONAL INFORMATION

Supplementary information The online version contains supplementary material available at https://doi.org/10.1038/s41524-023-01151-z.

Correspondence and requests for materials should be addressed to Yee Sin Ang or Chun Zhang.

Reprints and permission information is available at http://www.nature.com/reprints

Publisher's note Springer Nature remains neutral with regard to jurisdictional claims in published maps and institutional affiliations.